FISEVIER

Contents lists available at ScienceDirect

Thin Solid Films

journal homepage: www.elsevier.com/locate/tsf



Synthesis and Characterization

A comprehensive material study of CdSeTe films deposited with differing selenium compositions



Adam Danielson ^{a,*}, Carey Reich ^a, Jennifer Drayton ^b, Alexandra Bothwell ^{b,1}, Tushar Shimpi ^{a,2}, James Sites ^b, Walajabad Sampath ^a

- ^a Department of Mechanical Engineering, Colorado State University, Fort Collins, CO, 80538, United States
- b Department of Physics, Colorado State University, Fort Collins, CO, 80538, United States

ARTICLE INFO

Keywords:
Photovoltaics
Cadmium telluride
Cadmium selenide telluride
Photoluminescence
Close-space sublimation

ABSTRACT

The addition of selenium into CdTe to create the ternary alloy CdSeTe has been one of the most impactful advancements to CdTe-based photovoltaics in the last decade. CdSeTe/CdTe bilayer device structures have enabled a gain in short-circuit current due to the narrower bandgap of the alloy, with minimal to no loss in voltage. Intensity of photoluminescence and time-resolved photoluminescence measurements suggest this is due to an increase in carrier lifetime and concomitant greater fraction of radiative vs non-radiative recombination events which allows for a reduction in the voltage deficit. Here, we study the properties of as-deposited and CdCl2-treated CdSeTe films deposited by close-space sublimation under varying conditions from CdSeTe source charges with both 20 and 40 mol% CdSe. We find that the selenium content in the deposited films are substantially reduced from that of the source material. Additionally, deposition temperature, particularly that of the substrate, considerably affects the grain size, crystallinity, and photoluminescence of the material, illustrating the importance of source material selection and process optimization. Finally, we present evidence that the source material, and therefore the properties of the deposited films, change over time as the source material is used.

1. Introduction

Cadmium telluride (CdTe)-based solar cells are the second-most prolific photovoltaic (PV) technology today, currently exceeding 6 GWp of annual module production and continuing to rapidly expand [1]. With the ability to be manufactured using rapid deposition techniques such as close-space sublimation (CSS) or vapor transport deposition, utility-scale CdTe is the amongst the cheapest PV technology in terms of Levelized Cost of Energy and has reached parity or beaten conventional energy generation methods in terms of cost [2]. Additionally, as a material with a direct bandgap near the ideal for terrestrial applications, only a few micrometers of material is required to harvest much of the energy from the AM1.5 spectrum [3].

Arguably the most impactful advancement to CdTe-based technology within the past decade has been the inclusion of selenium into the illuminated side of the absorber to create a CdSeTe alloy. The bandgap of CdSeTe varies depending on the selenium composition. From a

bandgap of 1.5 eV as CdTe, the bandgap shrinks to a minimum of 1.37 eV at approximately 40% CdSe, then grows with increasing selenium as the bandgap approaches that of pure CdSe at 1.7 eV, described as "band bowing" [4, 5]. Typically, selenium concentrations corresponsing to a bandgap of 1.37-1.42 are used in PV devices which allows for increased current collection from lower energy photons compared to that of a \sim 1.5 eV CdTe absorber. This has led to a substantial increase in device short circuit current density [6]. Selenium has also been shown to passivate CdTe grains and grain boundaries [7] and drastically increases the minority carrier lifetimes within the absorber. Wheras a CdTe absorber typically exhibits a time-resolved photoluminescence tail lifetime of only a few nanoseconds, this increases to 25-50 ns in CdSe-Te/CdTe bilayer absorbers, and to hundreds of nanoseconds up to several microseconds in CdSeTe-only absorbers [6, 8, 9]. This increased passivation allowed for the voltage to remain unchanged despite the reduced bandgap, indicating a reduction in the voltage deficit from the theoretical limit. Yet despite its crucial role in modern CdTe-based solar

E-mail address: adam.danielson1@gmail.com (A. Danielson).

^{*} Corresponding author.

¹ Dr. Bothwell's present address is National Renewable Energy Laboratory, 15013 Denver West Parkway, Golden, CO, 80401, United States.

² Dr. Shimpi's present address is First Solar, 28101 Cedar Park Blvd, Perrysburg, OH, 43551, United States.

A. Danielson et al. Thin Solid Films 768 (2023) 139684

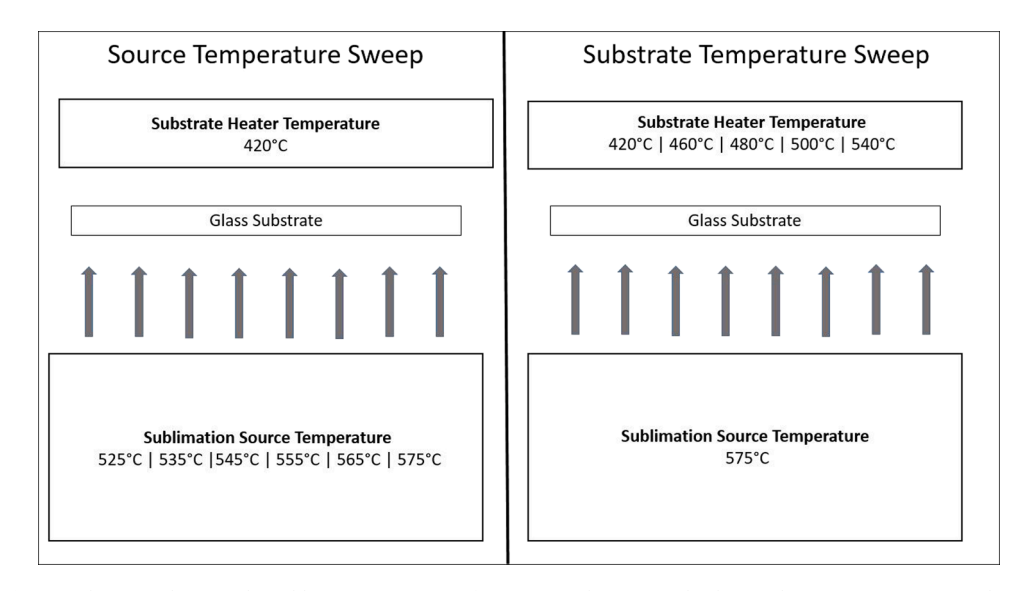


Fig. 1. Schematic showing the sublimation source configuration and source and substrate heater temperatures explored.

cells, relatively little has been published describing the properties of as-deposited and CdCl₂-treated CdSeTe.

Selenium is commonly alloyed into the CdTe absorber to create a graded CdSeTe bilayer using one of two methods. In the first, a thin layer of approximately 150 nm of CdSe is deposited directly on the electron contact, such as was done in [10]. A layer of CdTe is then deposited behind the CdSe, and the two layers are blended together during the CdCl₂ treatment. In the second method, a front layer of CdSeTe is deposited, usually by evaporation or sublimation (as in this study), from a mixture of CdSe and CdTe pre-prepared to contain a certain percentage of CdSe. Similar to the first method, when a full device is desired, a layer of CdTe is deposited behind the CdSeTe, and the selenium is diffused during CdCl₂. Both methods result in a graded bilayer with relatively high amounts of selenium at the front interface followed by a gradual decrease in selenium following a diffusion gradient until the absorber is nominally CdTe at an approximate depth of 1–1.5 µm [10, 11].

In this contribution, we study the material and optical properties of thin films sublimated from $CdSe_xTe_{1-x}$ source material with both x = 0.2and 0.4. Sensitivity to fabrication temperatures was investigated through deposition of films at varied source and substrate temperatures. Utilizing inductively-coupled plasma mass spectrometry and X-ray diffraction, we show that the selenium composition of the films is lower than in their respective source materials. We demonstrate that photoluminescence and film crystallinity are considerably affected by these deposition conditions. CdSe_{0.4}Te_{0.6} is found to be particularly sensitive to deposition conditions, as both cubic and hexagonal phases are seen at lower substrate temperatures, wheras $CdSe_{0.2}Te_{0.4}$ remains cubic throughout the substrate temperature sweep. Finally, analysis of the deposition rate, and scanning electron microscopy images reveal that the source material is not stable as it is used, and the amount of source material use drastically affects the film morphology. This work highlights the necessity of a well-understood and precisely-controlled CdSeTe layer for continued CdTe PV device performance advancement.

2. Experimental details

2.1. Sample fabrication

The films in this study were deposited on commercially available TEC10 glass substrates consisting of soda-lime glass with a SnO₂:F transparent conducting oxide (TCO) deposited on a sodium diffusion barrier. 100 nm of $Mg_xZn_{1-x}O$ (MZO) was magnetron sputter deposited on the TCO-side of the glass substrate. MZO is used as the electron

contact for full CdTe-based devices fabricated at Colorado State University. Although this study did not utilize full devices, the films were deposited on MZO in order to produce CdSeTe growth conditions that are representative of typical fabrication processes. The MZO was deposited at 140 W RF power across a 10.2 cm diameter oxide target composed of 11 wt% MgO and 89 wt% ZnO. Sputtering was performed in a 3% O₂/balance argon environment maintained at 0.66 Pa.

After a vacuum break, the samples were transferred to a multi-station vacuum chamber that allowed for all subsequent heating, absorber deposition via CSS, and CdCl2 treatments to be performed without breaking vaccum. A diagram and description of the chamber can be found in [12]. The substrates were preheated to 530 °C and then immediately transferred to one of several absorber deposition stations. Separate stations contained either a CdSe_{0.2}Te_{0.8} (CST20) or a CdSe_{0.4}Te_{0.6} (CST40) source material. The source materials were 5 N pure and prepared by 5 N Plus from a melt of the appropriate proportions of CdTe and CdSe. Absorbers were sublimated in a 5.3 Pa environment that was 2% O2/balance nitrogen. The depositons were performed as part of one of two temperature sweeps. In the first, a source temperature sweep, the substrate heater temperature was maintained at 420 °C while the source material temperature was swept from 525 °C to 575 °C in 10 °C increments. For the second sweep, a substrate heater temperature sweep, the source temperature was set at 575 °C while the substrate heater temperature was swept from 420 °C to 540 °C. Fig. 1 summarizes the conditions explored during this study. The substrate heater is located approximately a centimeter above the substrate during the film deposition. Film thicknesses were between 500 nm and 2 μ m, with the thinner samples used for transmission measurements and the thicker samples used for all other measurements. Samples annotated as "CdCl2-treated" received a 150-second CdCl2 treatment where the source and substrate heater temperatures were maintained at 440 $^{\circ}\text{C}$ and 387 $^{\circ}\text{C}$ respectively followed by a 240-second anneal at 400 $^{\circ}\text{C}.$

2.2. Characterization

2.2.1. Film thickness

The film thickness was measured using a Tencor Instruments Alpha Step 10-00,020 stylus profilometer. The film was manually scratched away down to the MgZnO and the stylus was scanned across the full width of the scratch. The step height was measured and divided by the dwell time in the deposition source to calculate the deposition rate.

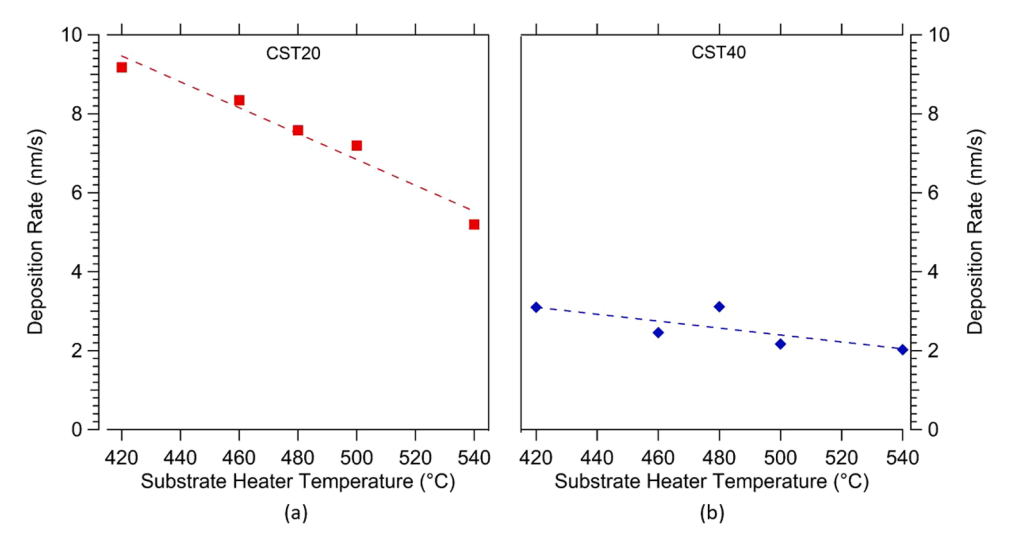


Fig. 2. Comparison of (a) CST20 and (b) CST40 deposition rates as a function of substrate heater temperature. The lines are guides to the eye.

2.2.2. Glancing angle X-ray diffraction

Glancing Angle X-ray Diffraction measurements were performed using a Bruker D8 Discover Series II equipped with an $CuK\alpha1$ X-ray source of 1.54 Å wavelength, a parabolic Göbel mirror and $^{1}\!\!\!/\!\!\!$ -circle Eulerian cradle. The angle was scanned from 5 to 80° in increments of 0.05° for the CST40 and from 20 to 80° in increments of 0.02° for the CST20. Peak positions and intensities were obtained using a Gaussian fit. Peaks were compared to Internation centre for Diffraction Data cards of various compositions of CdSeTe.

2.2.3. Photoluminescence emission spectroscopy

Photoluminescence (PL) measurements were conducted using glass-side excitation from a 520 nm laser using a Sony ILX511 CCD detector. A 570 nm long pass filter was installed between the sample and detector to minimize signal originating from the excitation laser.

2.2.4. Inductively coupled plasma-mass spectrometry

Inductively Coupled Plasma-Mass Spectrometry (ICP-MS) was performed by ALS Global using propriety methods. Approximately 1 cm² samples of CdSeTe films deposited on MgZnO and the Tec10 glass substrate were provided for analysis. Elemental compositions were reported as weight of the element per weight of the sample and converted to molar percentages.

2.2.5. Optical transmission

Optical transmission measurements were completed using PerkinElmer UV/Vis Lambda 2 Spectrometer equipped with both halogen and deuterium lamps. Optical bandgaps were calculated using the Tauc plot method where the linear portion of the $(\alpha h \nu)^2$ vs photon energy plot was extrapolated to the intercept with the abscissa [13].

2.2.6. Scanning electron microscopy

Scanning Electron Microscopy (SEM) images were obtained using a JEOL JSM-6500F field emission scanning electron microscope equipped with a Gatan CCD camera. Accelerating voltages were maintained between 10 and 15 kV and the working distance was kept between 9 and 10 mm.

3. Results and discussion

3.1. Deposition rate

To determine how the deposition rate of CdSeTe was affected by both the source temperature and the substrate temperature, numerous films were fabricated. Fig. 2 shows the deposition rate for both materials as the substrate heater temperature is increased from 420 to 540 $^{\circ}$ C. Both materials exhibit a relatively linear decrease in deposition rate as the

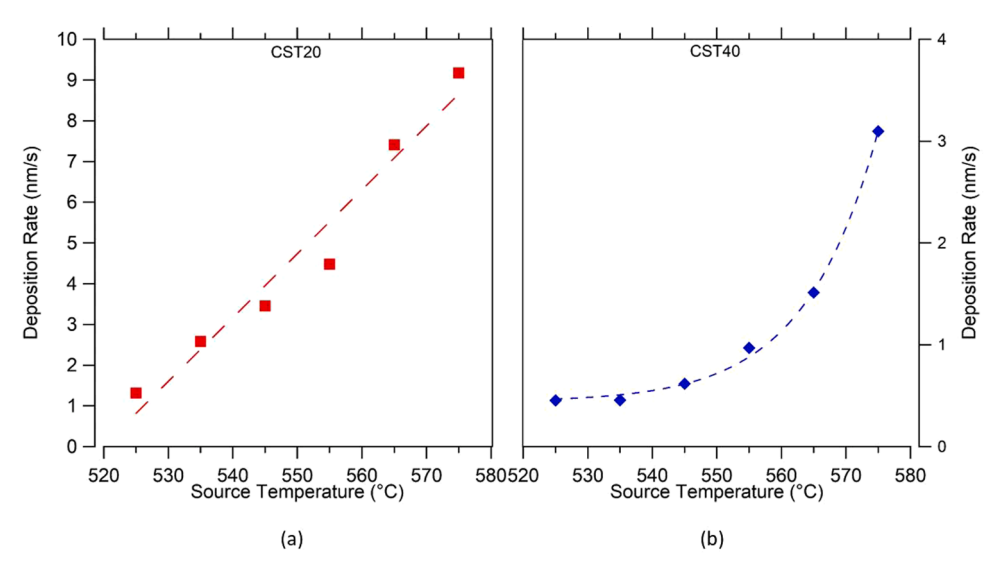


Fig. 3. deposition rates as a function of source temperature, for (a) CST20 and (b) CST40. Both show an exponential response to increasing source temperature.

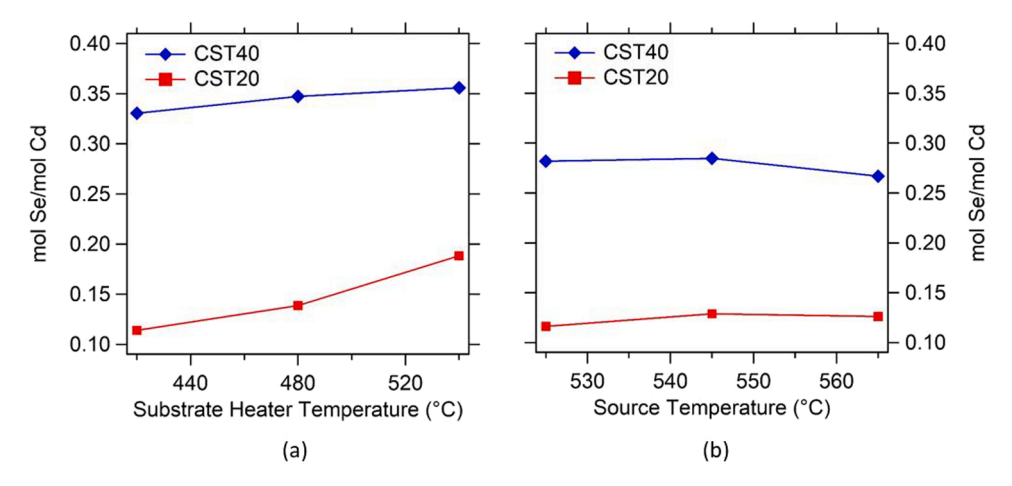


Fig. 4. ICP analysis showing selenium composition of films deposited with varying substrate (a) and source (b) temperatures. The lines are guides to the eye.

substrate temperature is increased. This is expected behavior due to increased desorption which occurs at the surface and the increased critical nucleation size required on the substrate [14]. While the deposition rate of both materials drop as the substrate temperature rises, the rate for CST20 remains 2–3 times that of CST40. The lower proportion of CdSe paired with the fact that CdTe has a greater vapor pressure than CdSe in these temperature ranges likely accounts for the higher deposition rate of CST20 [15].

Fig. 3 illustrates the deposition rate response to increasing source temperature. The two materials display similar exponential behavior and the difference between the two lies in the strength of the response. This response is expected, as vapor pressure also exponentially rises with temperature. Whereas CST20 exhibits a weak exponential dependence on source temperature and higher deposition rates, the response of CST40 is much stronger and deposition rates smaller. Once again, the increased proportion of CdSe in CST40 likely drives this difference in behavior. The deposition rate is comparitively reduced in CST40 at lower temperatures due to the high proportion of CdSe, but as the temperature increases, the deposition rate quickly increases. Beyond approximately 560 °C, even small source temperature changes result in large differences in deposition rate. The sensitivity of CdSeTe deposition rates, particularly that of CST40, to temperature must be accounted for to ensure the reliable and optimized fabrication of these films.

3.2. Selenium incorporation and film crystallinity

It is difficult to overstate how beneficial the inclusion of selenium has been to CdTe photovolatics. Increases in short circuit current, luminescence, and carrier lifetime [16] have all been attributed to selenium, as well as a sizable decrease in the voltage deficit [17]. Therefore, a critical aspect of depositing from a CdSeTe source is understanding the incorporation of selenium into the film as a function of the deposition conditions. The films were analyzed using ICP-MS, the results of which are shown in Fig. 4a (substrate temperature sweep) and 4b (source temperature sweep.)

Increasing the substrate heater temperature during depositon from 420 $^{\circ}\text{C}$ to 540 $^{\circ}\text{C}$ results in a minor increase in selenium incorporation from 0.33 to 0.36 mol Se/mol Cd in CST40, a 9.1% relative increase, but a much more pronouced 72.7% relative increase from 0.11 to 0.19 mol Se/mol Cd in CST20. Alternatively, increasing the source temperature does not appear to significantly impact selenium incorporation in either material. A notable finding is that for both materials and all conditions tested, the selenium content in the deposited film is less than that of the source material. Only 55–70% of the selenium present in the source material incorporates into the film, depending on the deposition temperatures. So the terms "CST20" and "CST40" are appropriate names to describe the source material, but are misleading when describing the

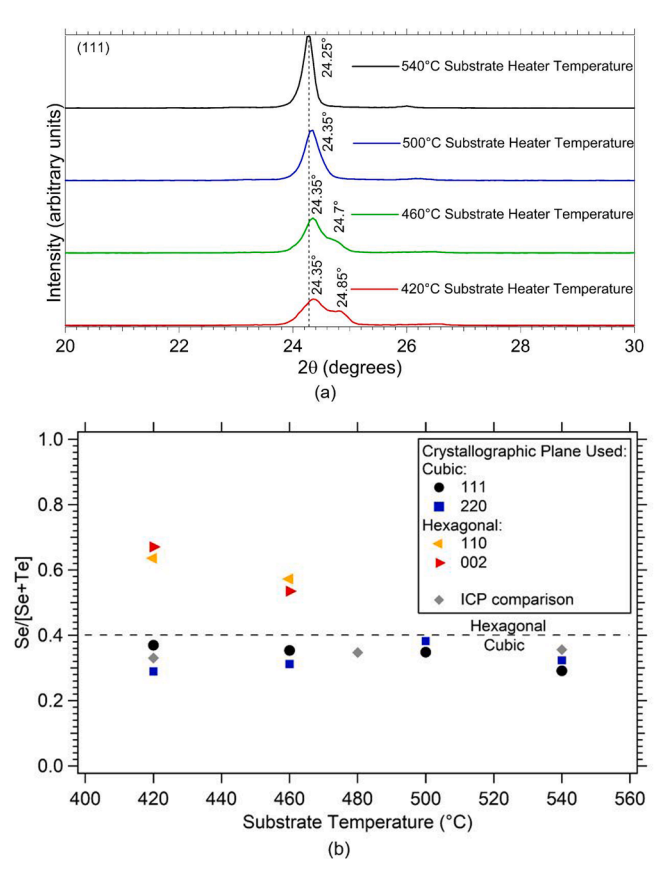


Fig. 5. (a) XRD measurements of as-deposited CST40 shows the reduction of the hexagonal peak and strengthening cubic peak as substrate temperature increases. The vertical dashed corresponds with the 540 $^{\circ}$ C peak to aid in visualizing the peak shift. (b) A comparison of the selenium composition of the cubic and hexagonal phases within CST40, as determined by a fit of the lattice parameters.

actual selenium concentration in deposited films.

To study the crystalline structure of the as-deposited films, X-ray diffraction measurements were taken on films deposited with differing substrate temperatures. Fig. 5a shows the resulting data for as-deposited CST40. In this figure, each fit peak location is annotated above the curve, and a vertical dashed black line is centered on the 540 $^{\circ}$ C peak location to highlight the peak shift between samples.

It is apparent from the XRD patterns that the deposited film forms

A. Danielson et al. Thin Solid Films 768 (2023) 139684

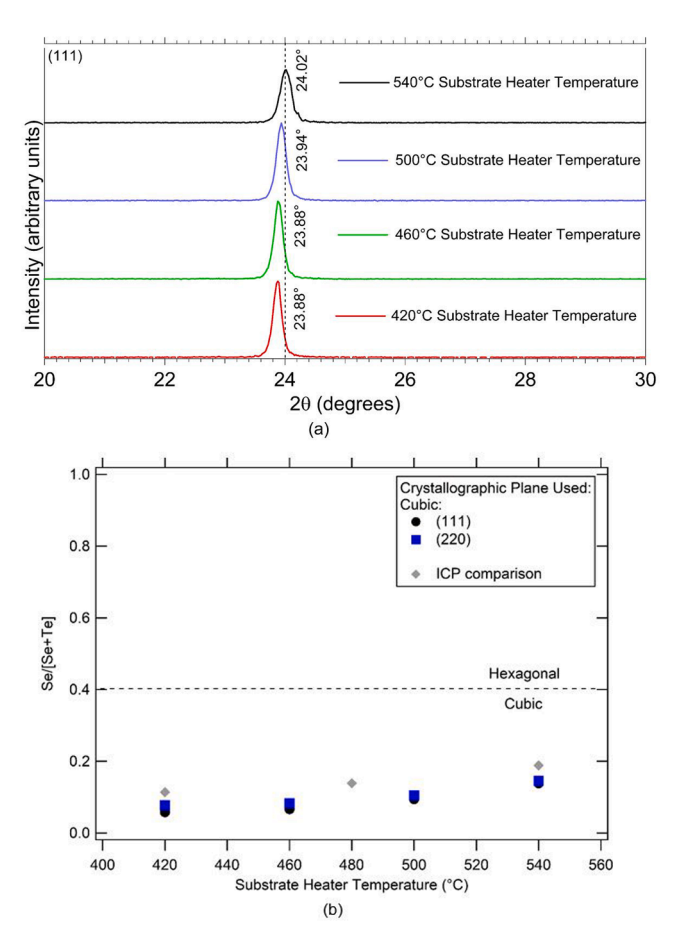


Fig. 6. (a) XRD data for as-deposited CST20 as the substrate temperature increases. Single cubic peaks are observed at all substrate heater temperatures. The vertical dashed line corresponds to the $540\,^{\circ}\text{C}$ peak and is used as an aid in visualizing the peak shift. (b) A comparison of the selenium composition of the cubic phase in CST20, determined by a fit of the lattice parameters to the composition as determined by ICP-MS.

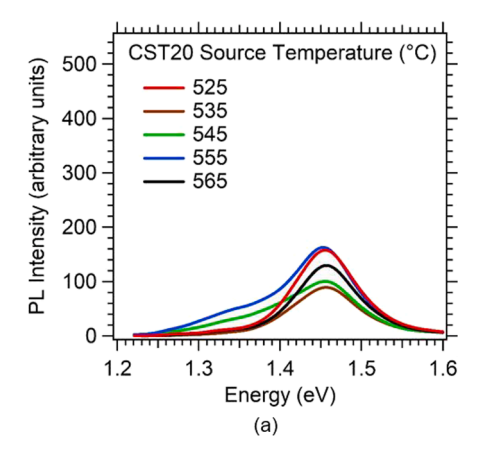
two sets of peaks at lower substrate temperatures corresponding to the cubic (111) and hexagonal (002) phases, but a single cubic peak at higher substrate temperatures. Using XRD cards of the CdTe-CdSe solid solution we fit the lattice parameter a_0 for the cubic phase and the lattice parameters a and c for the hexagonal phases [18–21]. Based on these fits and determination of the lattice constants using the cubic (111) and (220) planes and the hexagonal (002) and (110) peaks, composition for the different phases was calculated and compared to the ICP-MS

determined composition. The comparison is shown in Fig. 5b. First, it is apparent that the hexagonal phase has a selenium composition between x=0.5 and x=0.7, decreasing with the increased substrate heater temperature but always drastically greater than that of the cubic phase material. Additionally, it is clear that the volume fraction of these hexagonal phases is small, since the ICP-MS data agree with the compositions determined by the cubic phase, approximately x=0.3 to 0.38. It is likely that the hexagonal phase is the result of poor adatom surface diffusion behavior leading to localized regions of higher selenium concentration during deposition.

As the substrate heater temperature is increased from 420 $^{\circ}$ C to 540 $^{\circ}$ C, the crystallinity markedly improves, as evidenced by the elimination of the hexagonal peak and reduction of the FWHM of the main cubic peak. At temperatures of 500 $^{\circ}$ C and greater, only the cubic phase is seen. Eliminating the hexagonal peak through the careful selection of deposition temperatures is crucial, as even minute amounts of hexagonal phase CdSeTe has been shown to drastically reduce device performance [22].

Fig. 6a and 6b show the XRD data and lattice parameter-fit selenium composition respectively for as-deposited CST20. They reveal that the main peak of CST20 occurs at a 2θ of approximately 23.9° , corresponding to the (111) peak of CdSe $_{0.1}$ Te $_{0.9}$ [23] . The trend of peak sharpening at higher substrate temperatures is not present in CST20 as it was in CST40. What is present is a prominent peak shift towards a higher 2θ as the substrate temperature increases, indicating a decrease in lattice parameter associated with an increase in selenium in the cubic phase. Both methods of determining selenium composition shown in Fig. 6b agree that the selenium incorporation increased at higher substrate temperatures and that the magnitude of change in selenium is substantially larger for CST20 than for CST40. With a substrate heater temperature of 540 °C, the (111) peak is located at just over 24° , shifting closer to the (111) peak of CdSe $_{0.2}$ Te $_{0.8}$ [24].

Finally, there is no indication of the hexagonal phase contributing to a double peak for any condition of CST20. Wheras CST40's composition places it near the transition point between cubic and hexagonal phase, CST20 lies comfortably within the regime where cubic crystalline structure formation is energetically favorable [25]. We therefore conclude that while 420 °C may be an appropriate substrate temperature for CST20 fabrication, it is suboptimal for CST40. It is also likely that when depositing with a substrate heater temperature greater than 460 °C, the films may require a less aggressive CdCl2 treatment to remove hexagonal-phase crystalites and achieve the full cubic-phase recrystallization, large grains, and chlorine passivation necessary for high performance solar cells.



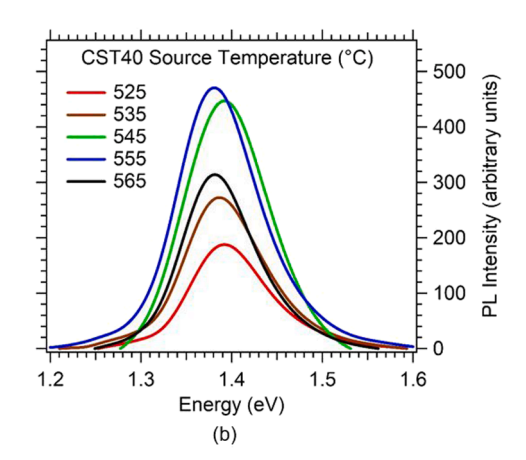
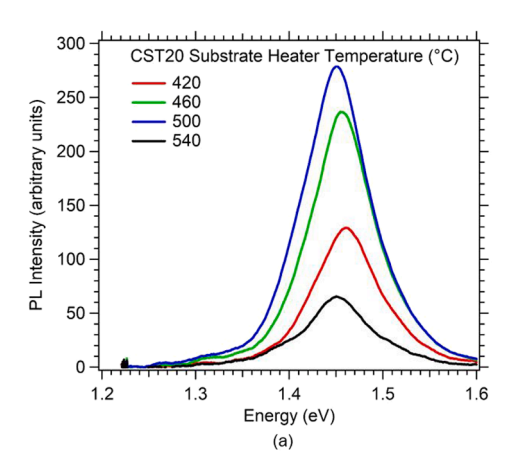


Fig. 7. Comparison of (a) CST20 and (b) CST40 steady state photoluminescence spectra when deposited with varying source temperature.



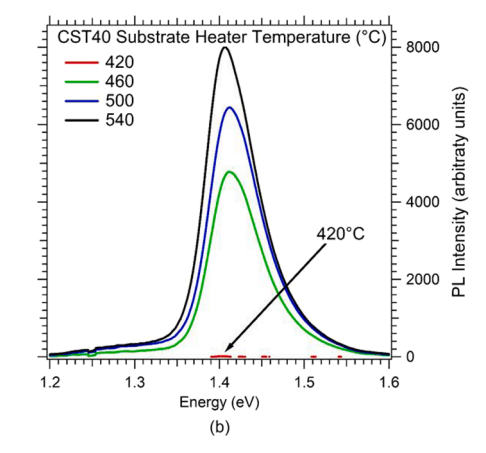


Fig. 8. Comparison of (a) CST20 and (b) CST40 steady state photoluminescence spectra when deposited with varying substrate temperatures.

3.3. Photoluminescence

Fig. 7a and b show the steady state photoluminescence spectra for CST20 and CST40, respectively, as the source temperature is increased. Data are only shown for CdCl2-treated samples, as no photoluminescence emission is observed in as-deposited films. CST40 is more luminescent than CST20 for all conditions tested, indicating a comparative reduction of defect-assisted recombination in CST40. This is in good agreement with past findings which show the passivating effects of selenium in CdTe films [7]. The peak locations are relatively constant as the source temperature changes, remaining between 1.45 and 1.46 eV for CST20 and between 1.39 and 1.40 eV for CST40. The narrower bandgap of CST40 aligns with the known bandgap "bowing" behavior that occurs in CdSeTe as the selenium proportion increases [4]. Both materials exhibit a maximum peak intensity at 555 °C source temperature, but the small differences in PL intensity shown here are unlikely to manifest as significant differences in current density vs. voltage (JV) performance. The PL data for CST20 reveal a second low-energy peak which is visible for several source temperatures. Similar sub-bandgap features and low energy peaks have been observed in CST40 and are typically attributed to band tails. These low energy peaks, which may at times be quite substantial, reduce the effective bandgap of the material and the implied voltage which the absorber can produce as reported in [9, 26]. Investigating the nature of these sub-bandgap features, and

minimizing them, is an important step in optimizing future CdSeTe solar cells.

Fig. 8a and b show the steady state PL for CST20 and CST40 as a function of substrate heater temperature. CST20 displayed increased PL intensity until 500 °C, at which point the PL decreased again. CST40 however, showed an increase in PL throughout the entire temperature sweep, up to a maximum at 540 °C. To highlight the temperature trends for both materials, Fig. 8a and b have been plotted on different PL intensity scales. Notably, where other PL comparisons in this study dealt with a 2–3x increase in PL signal, when the substrate heater temperature was increased for CST40, the PL improved greatly, exhibiting an increase of several orders of magnitude from 420 °C to 540 °C. Indeed, in Fig. 8b, the peak for 420 °C is barely visible at this scale. Increasing substrate temperature appears to discourage the formation of defects which facilitate non-radiative recombination.

3.4. Transmission and optical bandgap

The optical bandgap of both materials was determined utilizing transmission curve measurements and the Tauc plot technique [13]. This allowed for the confirmation of the bandgap values as approximated by PL peak location and was performed on films before and after the $CdCl_2$ treatment to quantify changes. The transmission curves for both materials are shown in Fig. 9 where the solid lines are as-deposited

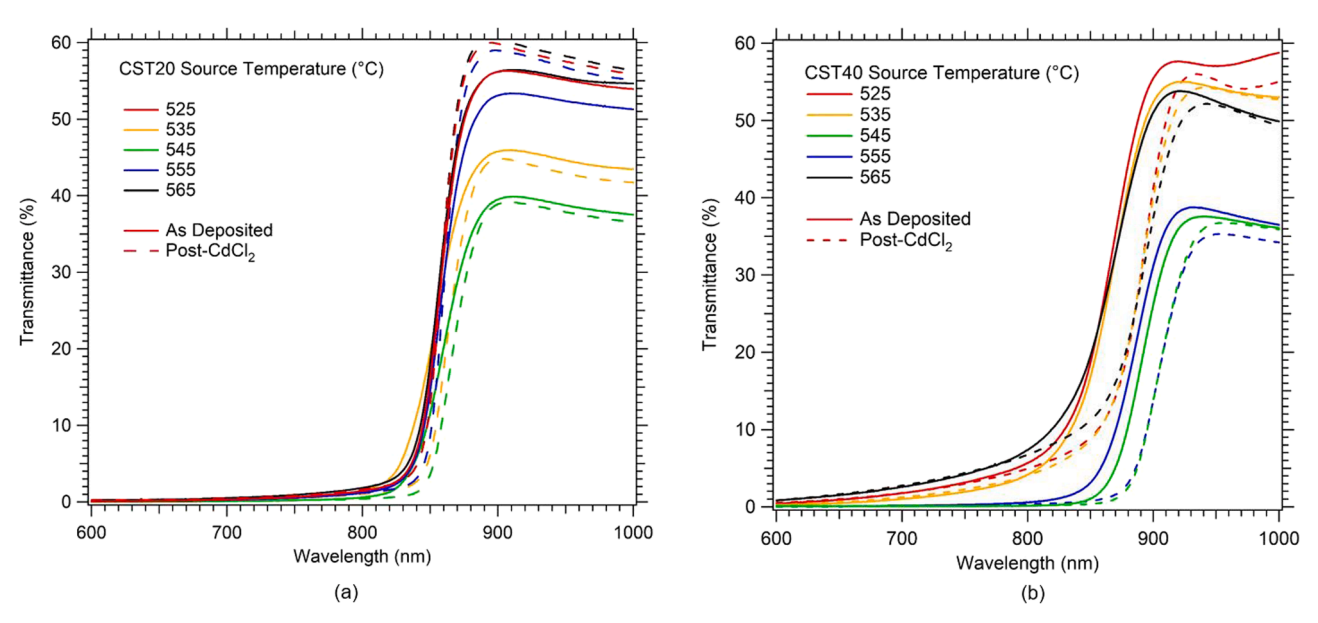


Fig. 9. Transmission curves of as-deposited and CdCl₂-treated (a) CST20 and (b) CST40 films.

Table 1
Bandgap measurements for as-deposited and CdCl₂-treated CST20 and CST40.

| Source Temperature (°C) | As-Deposited E _g (eV) | | CdCl ₂ Treated E _g (eV) | |
|--------------------------|----------------------------------|-------|---|-------|
| | CST20 | CST40 | CST20 | CST40 |
| 525 | 1.45 | 1.42 | 1.45 | 1.38 |
| 535 | 1.46 | 1.42 | 1.44 | 1.38 |
| 545 | 1.46 | 1.41 | 1.44 | 1.38 |
| 555 | 1.46 | 1.41 | 1.44 | 1.37 |
| 565 | 1.46 | 1.41 | 1.45 | 1.37 |

and the dashed are after the CdCl2 treatment.

Both materials demonstrated a decrease in bandgap after the $CdCl_2$ treatment for all conditions. The bandgap decreased from approximately 1.46 to 1.44 eV in CST20 and from approximately 1.42 to 1.38 in CST40

and are summarized in Table 1. This decrease can likely be attributed to selenium diffusion and the reduction or removal of hexagonal phase material during the recrystallization which occurs during the $CdCl_2$ treatment, particularly for CST 40, such as that shown in Fig. 5. Given an understanding of these changes, this may provide a route to manipulate the bandgap and could be harnessed to engineer device structures with an optical bandgap near 1.4 eV, optimal for absorbing the AM 1.5 spectrum.

3.5. Morphology and grain stucture

To conclude the study, the morphology and grain structure of each film were investigated using a scanning electron microscope. While all conditions were studied, a few images were selected which best

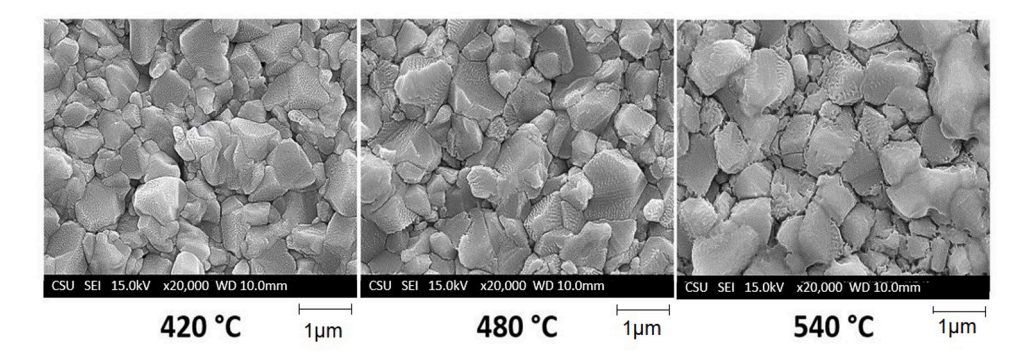


Fig. 10. SEM images of as-deposited CST20, showing columnar grain growth and increased grain size as substrate temperature increases.

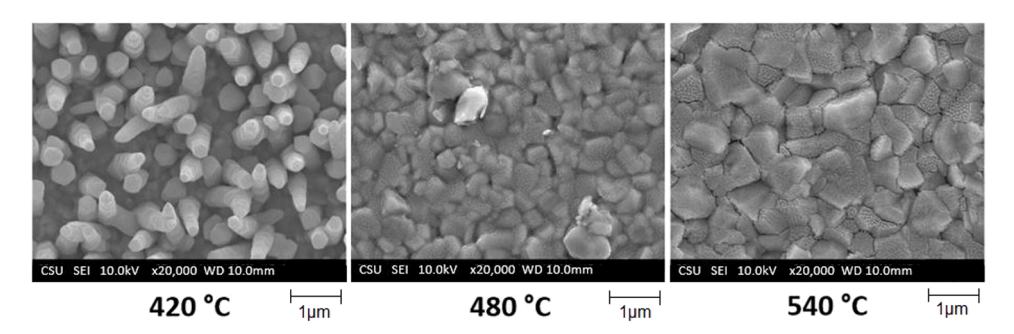


Fig. 11. SEM images of as-deposited CST40, showing extreme columnar growth occurring at lower substrate temperatures and larger, equiaxed grains at higher temperatures.

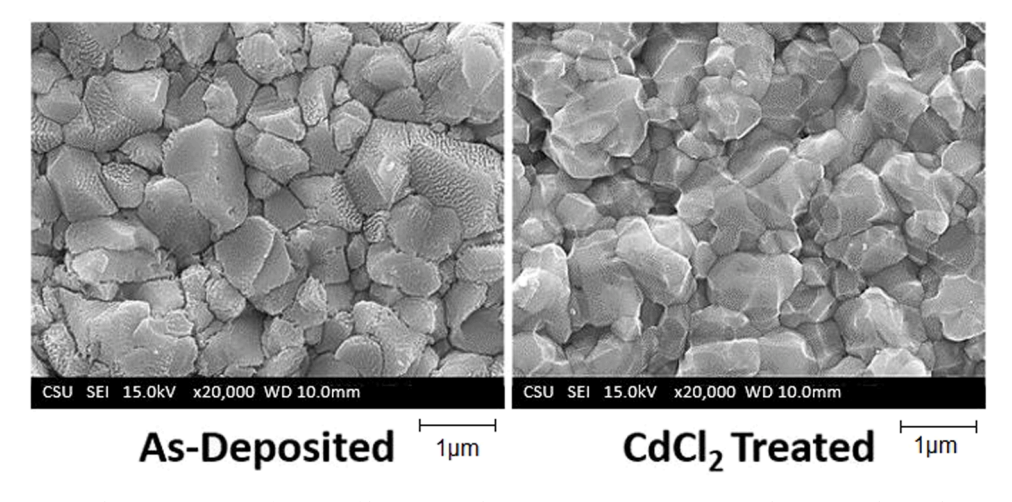


Fig. 12. SEM images comparing the grain structure of a CST20 film grown with a 575 °C source temperature and a 500 °C substrate heater temperature, before and after CdCl₂ treatment.

A. Danielson et al. Thin Solid Films 768 (2023) 139684

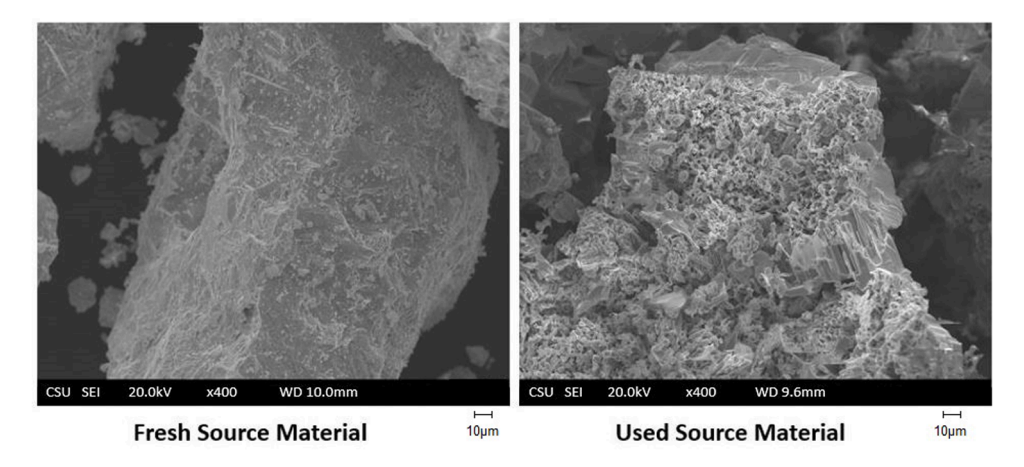


Fig. 13. SEM images comparing fresh CST40 source material with used source material. Significant pitting is observed in the used material.

illustrate the structural changes observed. No apparent structural changes were observed as the source temperature increased, and therefore are not presented in this work. The substrate temperature however, was shown to drastically affect the film morphology. Fig. 10 shows as-deposited CST20 films as a function of the substrate heater temperature. As the substrate temperature increases, the grains become larger and more equiaxed. These large, equiaxed grains are the result of increased surface and bulk diffusion, facilitated by the increased substrate temperature and predicted by standard structure-zone models, such as is presented in [14].

Fig. 11 shows the same conditions for CST40. Although the same basic trend of increased grain size is noted, the change is far more drastic. Particularly the 420 °C condition deserves discussion. This film displays grains that have formed in tall, steep-sided pillars, indicating that this film's growth conditions were firmly within the columnar growth regime, where adatoms lack sufficient mobility to diffuse along the surface [14]. It must be noted that this is the deposition condition used in many high efficiency (18–20%) CdSeTe/CdTe bilayer devices made at Colorado State University. Examples can be found in [27]. The large aspect ratio of these pillars likely causes shadowing during deposition, preventing the CdTe, which is deposited immediately following the CdSeTe, from making intimate contact with the preceding layer in all locations. Then during the CdCl₂ treatment, as the grains restructure and grow, the voids coalesce such as those observed using transmission electron microscopy and cathodoluminescence [7, 28].

The CdCl₂ treatment process is critically important to fabricating functioning CdTe photovoltaic devices. During this treatment, stacking faults and defects are eliminated and chlorine diffuses into the absorber, passivating grain boundaries and interfaces [28–30]. Fig. 12 compares the film structure of a CST20 film, chosen as an exemplar, before and

after the $CdCl_2$ treatment. Further grain growth and a less faceted appearance result from the merging of grain boundaries which occurs during recrystallization.

3.6. Source material instability

One significant consequence of depositing from a CdSeTe source is that the material is not stable throughout its life. As the material is used, the composition of the source material appears to change. SEM images of fresh and used CST40 source material shown in Fig. 13 highlight the pits and "pockets" which form in the source material as it is used. This pitting is likely an indication of preferential sublimation resulting from small compositional variations in the source material [31].

We observe a significant decrease in source material deposition rate which appears to be time-of-use dependent. The deposition rates of these materials may vary substantially depending on the age of the material compared to what we have earlier shown. Fig. 14 shows the deposition rate variation for both CST20 and CST40, which was measured over several months while using the same deposition conditions. In this figure, the number of days which have elapsed is used as a reasonable proxy for total time of use as the average daily time of use is relatively consistent. The thick vertical lines represent when the sublimation source material was replaced. Both materials exhibit a similar behavior in which the deposition rate peaks with fresh material, and gradually declines with use. Both materials appear to eventually reach a critical threshold of use where the deposition rate drops precipitously, reaching a low of less than 40% of the original rate. Alternatively, if the material is replaced with reasonable frequency, the deposition rate can be maintained at approximately 70% or more of the maximum. Since we have shown that CdSeTe materials with differing Se content exhibit

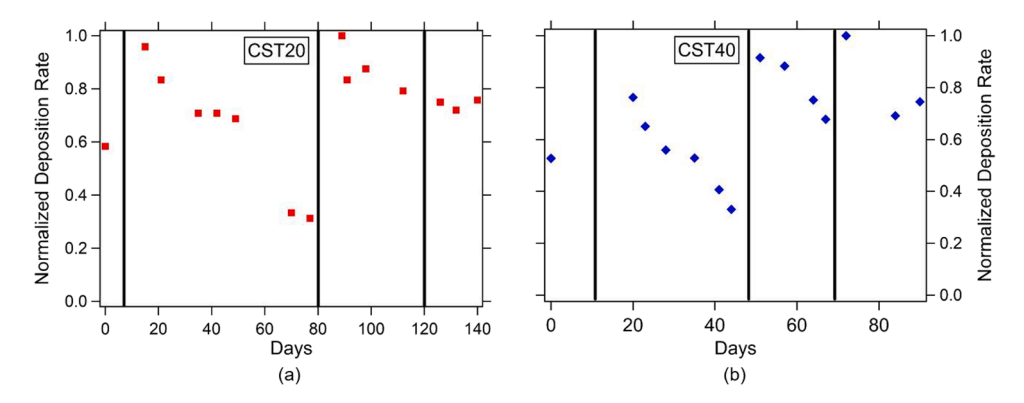


Fig. 14. Normalized deposition rate of CST20 (red) and CST40 (blue) showing a decrease over time. The black vertical lines represent where the material was replaced.

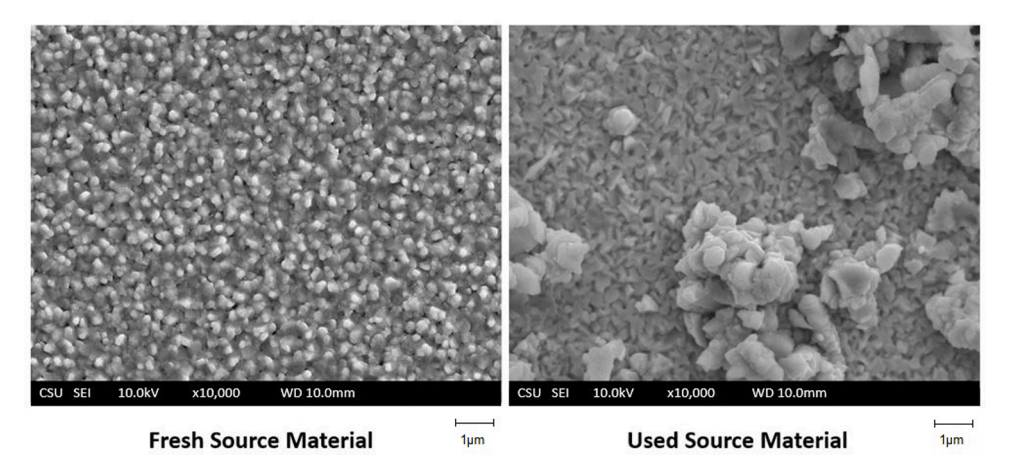


Fig. 15. SEM images showing changes in the film morphology between CST40 films fabricated using fresh source material (left) and old source material (right).

different deposition rates, we hypothesize that the drop in deposition rate corresponds with preferential sublimation of CdTe and a progressively Se-rich source material.

Finally, evidence of the changing source material can also be seen in SEM images of as-deposited films. Fig. 15 is a side-by-side comparison of two CST40 films which were fabricated using the same deposition conditions. The film on the left was fabricated using fresh source material, while that on the right was fabricated with material after it had been maintained at sublimation temperatures for approximately 160 h. These images illustrate how drastically the morphology of the film may be affected by the age of the source material. This adds to the growing body of evidence indicating that these source materials are subject to changing deposition characteristics over the lifetime of the source material and caution needs to used when determining the useful life of these source charges.

4. Conclusion

In summary, we examined the properties of CdSeTe thin films when deposited by the sublimation of varying source materials. We have shown that the selenium incorporation within the films is notably lower than within the source material. Furthermore, we have illustrated how these materials' deposition rate, crystallinity, luminescence, band-gap and grain morphology are affected by deposition conditions and selenium concentration. Substantial changes in the grain structure and properties of CST40 are noted as a function of changing temperatures. Finally, we have observed that the properties of the deposited films change as the source material is continually used over hundreds of hours, likely indicating that the composition of the source materials changes with time. This work demonstrates the importance of a wellunderstood, well-optimized CdSeTe fabrication process. Given the foundational role that CdSeTe now plays in CdTe-based PV devices, such knowledge will promote future targeted device engineering and improved efficiencies.

CRediT authorship contribution statement

Adam Danielson: Conceptualization, Methodology, Investigation, Writing – original draft, Visualization. Carey Reich: Conceptualization, Methodology, Investigation, Writing – review & editing, Visualization. Jennifer Drayton: Conceptualization, Methodology, Investigation, Writing – review & editing, Visualization. Alexandra Bothwell: Conceptualization, Methodology, Investigation, Writing – review & editing, Visualization. Tushar Shimpi: Investigation. James Sites: Funding acquisition. Walajabad Sampath: Funding acquisition.

Declaration of Competing Interest

The authors declare the following financial interests/personal relationships which may be considered as potential competing interests: Adam Danielson reports financial support was provided by US Department of Energy. Adam Danielson reports financial support was provided by National Science Foundation. Adam Danielson reports equipment, drugs, or supplies was provided by 5NPlus Inc. Tushar Shimpi reports a relationship with First Solar Inc that includes: employment.

Data Availability

Data will be made available on request.

Acknowledgments

This material was partially based upon work supported by the U.S. Department of Energy's Office of Energy Efficiency and Renewable Energy (EERE) under Solar Energy Technologies Office (SETO) Agreement number DE-EE0008557 and DE-EE0008552. The authors would also like to acknowledge the support from the National Science Foundation under the Industry/University Cooperative Research Center (I/UCRC) for Next Generation Photovoltaics program (Award numbers – 1821526 and 2052735), and the I/UCRC for Next Generation Photovoltaics Industrial Advisory Board. All the CdSeTe and CdCl₂ used in this work were supplied by 5N Plus Inc. The authors wish to thank the Analytical Resources Core (RRID:SCR_021758) at Colorado State University for instrument access, training and assistance with sample analysis.

References

- I. FRAUNHOFER INSTITUTE FOR SOLAR ENERGY SYSTEMS, Photovoltaics Report 2021, 2021.
- [2] Lazard, Lazard's Levelized Cost of Energy Analysis Version 15.0, 2021, pp. 0–20.
- [3] B.E. M.ccandless, J.R. S.ites, Cadmium Telluride Solar Cells, in: S. Hegedus, A. Luque (Eds.), Handbook of Photovoltaic Science and Engineering, 2003, pp. 617–662.
- [4] N. Muthukumarasamy, S. Jayakumar, M.D. K.annan, R. Balasundaraprabhu, Structural phase change and optical band gap bowing in hot wall deposited CdSexTe1-x thin films, Sol. Energy 83 (4) (2009) 522–526, https://doi.org/ 10.1016/j.solener.2008.10.004.
- [5] D.E. S.wanson, J.R. S.ites, W.S. S.ampath, Co-sublimation of CdSexTe1-x layers for CdTe solar cells, Sol. Energy Mater. Sol. Cells 159 (2017) 389-394, https://doi. org/10.1016/j.solmat.2016.09.025.
- [6] A.H. M.unshi, et al., Polycrystalline CdSeTe/CdTe absorber cells with 28 mA/cm2 short-circuit current, IEEE J. Photovolt. 8 (1) (2018) 310–314, https://doi.org/ 10.1109/JPHOTOV.2017.2775139.

- [7] T.A.M. Fiducia, et al., Understanding the role of selenium in defect passivation for highly efficient selenium-alloyed cadmium telluride solar cells, Nat. Energy 4 (6) (2019) 504–511, https://doi.org/10.1038/s41560-019-0389-z.
- [8] J.M. K.ephart, et al., Sputter-deposited oxides for interface passivation of CdTe photovoltaics, IEEE J. Photovolt. 8 (2) (2018) 587–593, https://doi.org/10.1109/ JPHOTOV.2017.2787021.
- [9] A. Onno, et al., Understanding what limits the voltage of polycrystalline CdSeTe solar cells, Nat. Energy (2022), https://doi.org/10.1038/s41560-022-00985-z.
- [10] T. Ablekim, et al., Thin-Film Solar Cells With 19% Efficiency by Thermal Evaporation of CdSe and CdTe, 2020, https://doi.org/10.1021/ acsenersylett 9h02836
- [11] A.H. Munshi, A.H. Danielson, K.L. Barth, G. Gelinas, J.N. Beaudry, W.S. Sampath, Advanced co-sublimation of low bandgap CdSex Te1-x alloy to achieve higher short-circuit current, in: 2018 IEEE 7th World Conf. Photovolt. Energy Conversion, WCPEC 2018 - A Jt. Conf. 45th IEEE PVSC, 28th PVSEC 34th EU PVSEC, 2018, pp. 148–152, https://doi.org/10.1109/PVSC.2018.8548272.
- [12] D.E. S.wanson, et al., Single vacuum chamber with multiple close space sublimation sources to fabricate CdTe solar cells, J. Vac. Sci. Technol. A Vacuum, Surfaces, Film. 34 (2) (2016), 021202, https://doi.org/10.1116/1.4941071.
- [13] J. Tauc, Optical properties and electronic structure of amorphous Ge and Si, Mater. Res. Bull. 3 (1968) 37–46.
- [14] M. Ohring, Materials Science of Thin Films, Elsevier, 2001.
- [15] W.J. Wosten, The vapor pressure of cadmium selenide, J. Phys. Chem. 65 (11) (1961) 1949–1951, https://doi.org/10.1021/j100828a008.
- [16] A.M. B.othwell, J.A. D.rayton, P.M. J.undt, J.R. S.ites, Close-space sublimation-deposited ultra-thin CdseTe/CdTe solar cells for enhanced short-circuit current density and photoluminescence, J. Vis. Exp. 2020 (157) (2020) 1–10, https://doi.org/10.3791/60937.
- [17] D. Kuciauskas, et al., Voltage loss comparison in CdSe/CdTe solar cells and polycrystalline CdSeTe heterostructures, IEEE J. Photovolt. 12 (1) (2022) 6–10, https://doi.org/10.1109/JPHOTOV.2021.3117914.
- [18] H. Ben-Dor, L. Yellin, N. Shaham, Low temperature synthesis of pseudobinary chalcogenides, Mater. Res. Bull. 19 (4) (1984) 465–470, https://doi.org/10.1016/ 0025-5408(84)90107-7.
- [19] G. Vitrikhovskii, N. Mizetskaya, I. Oliinyk, Properties of alloys belonging to the system CdSe-CdTe, Inorg. Matterials 7 (1971) 657.

- [20] I.B. S.hevchenko, Y... Nikol'skii, E.M. S.tairnova, V.R. D.arashkevich, Y.E. S.utyrin, Solid solutions of the system CdSe-CdTe, Inorg. Mater. 10 (184) (1974).
- [21] J. Litwin, X-ray examination of the binary system CdTe-CdSe, Phys. Status Solidi 5 (3) (1964) 551–553, https://doi.org/10.1002/pssb.19640050311.
- [22] K.J. H.ayes, CdTe solar cell optimization by planar and transmission EBSD, Microsc. Microanayl. 2 (2016) 2–3.
- [23] S. Razik, N. Al-Barakati, G. Al-Heneti, Powder diffraction data of CdTexSe1-x solid solutions, Powder Diffr. 5 (4) (2013) 206–209, https://doi.org/10.1017/ S0885715600015815.
- [24] M.M. E.I-Nahass, M.M. S.allam, M.A. A.fifi, I.T. Z.edan, Structural and optical properties of polycrystalline CdSexTe1-x $(0 \le x \le 0.4)$ thin films, Mater. Res. Bull. 42 (2) (2007) 371–384, https://doi.org/10.1016/j.materresbull.2006.05.022.
- [25] J. Steininger, A.J. S.trauss, Phase diagrams and crystal growth of pseudobinary alloy semiconductors, J. Cryst. Grow. 13–14 (C) (1972) 657–662, https://doi.org/ 10.1016/0022-0248(72)00537-4
- [26] A. Onno, et al., Calculation of the thermodynamic voltage limit of CdSeTe solar cells, Conf. Rec. IEEE Photovolt. Spec. Conf. 2020-June (2020) 0535–0537, https://doi.org/10.1109/PVSC45281.2020.9300938.
- [27] T. Shimpi, et al., Influence of process parameters and absorber thickness on efficiency of polycrystalline CdSeTe/CdTe thin film solar cells, Conf. Rec. IEEE Photovolt. Spec. Conf. 2020-June (2020) 1933–1935, https://doi.org/10.1109/ PVSC45281.2020.9300840.
- [28] A.H. M.unshi, et al., Effect of CdCl2 passivation treatment on microstructure and performance of CdSeTe/CdTe thin-film photovoltaic devices, Sol. Energy Mater. Sol. Cell. 186 (June) (2018) 259–265, https://doi.org/10.1016/j. solmat 2018 06 016
- [29] S.H. Y.oo, K.T. B.utler, A. Soon, A. Abbas, J.M. W.alls, A. Walsh, Identification of critical stacking faults in thin-film CdTe solar cells, Appl. Phys. Lett. 105 (6) (2014) 1–5, https://doi.org/10.1063/1.4892844.
- [30] C. Li, et al., Grain-boundary-enhanced carrier collection in CdTe solar cells, Phys. Rev. Lett. 112 (15) (2014), 156103, https://doi.org/10.1103/ PhysRevLett.112.156103. Apr.
- [31] W. Callister, D. Rethwisch, Materials Science and Engineering-An Introduction, 8th ed., John Wiley & Sons, Inc., Hoboken, 2010.